Journal of Alloys and Compounds 644 (2015) 423–429

Contents lists available at ScienceDirect

Journal of Alloys and Compounds

journal homepage: www.elsevier.com/locate/jalcom

Thermal infrared and microwave absorbing properties of $SrTiO_3$/$SrFe_{12}O_{19}$/polyaniline nanocomposites

Seyed Hossein Hosseini [a,*], Parisa Zamani [b], S.Y. Mousavi [c]

[a] Department of Chemistry, Faculty of Science, Islamshahr Branch, Islamic Azad University, Tehran, Iran
[b] Department of Applied Chemistry, Faculty of Pharmaceutical Chemistry, Pharmaceutical Sciences Branch, Islamic Azad University, Tehran, Iran
[c] Faculty of Passive Defense, Imam Hossein University, Tehran, Iran

ARTICLE INFO

Article history:
Received 10 April 2015
Received in revised form 2 May 2015
Accepted 11 May 2015
Available online 16 May 2015

Keywords:
Magnetic nanoparticle
Nanocomposite
Polyaniline
Microwave absorption
Thermal IR absorption

ABSTRACT

Polyaniline (PANI) as a unique polymer that also has electromagnetic absorption used as the substrate. In this research, $SrTiO_3$ was synthesized as IR absorbent and core and then $SrFe_{12}O_{19}$ as microwave absorbent was prepared on $SrTiO_3$ via co-precipitation method as the first shell. As the next step, PANI was coated on $SrTiO_3$/$SrFe_{12}O_{19}$ nanoparticles via in situ polymerization by multi core–shell structures ($SrTiO_3$/$SrFe_{12}O_{19}$/PANI). Nanometer size and structures of samples were measured by TEM, XRD and FTIR. Morphology of nanocomposite was showed by SEM images. The magnetic and electric properties were also performed by VSM and four probe techniques. Thermal infrared (IR) absorption and microwave reflection loss of nanocomposites were investigated at 10–40 μm and 8–12 GHz, IR and microwave frequencies, respectively. The results showed that the $SrTiO_3$/$SrFe_{12}O_{19}$/PANI nanocomposites have good compatible electric and magnetic properties and hence the microwave absorbency shows wide bandwidth properties. The infrared thermal image testing showed that the function of infrared thermal imaging was optimized by increasing $SrTiO_3$/$SrFe_{12}O_{19}$ as core and independent to increasing PANI as the final shell.

1. Introduction

Thermal infrared radiation is much commonly known as kind of radiative heat. The thermal infrared region is the wavelength range of the electromagnetic spectrum which is also a characteristic of the thermal or heat radiation from the Earth's surface and from the atmosphere. In thermal equilibrium, the emission of radiation in the infrared is governed by Planck's law, which describes the spectral distribution of the energy emitted by "black" bodies (i.e. having unit emissivity at all wavelengths) as a function of temperature. Both the Earth's surface and the atmosphere emit in the so-called "thermal" infrared, having spectral distributions described by the Planck function corresponding to the local temperature, (i.e. the surface temperature of the Earth and the temperature as function of altitude.) Since the temperature of the Earth's surface is about 300 K, according to Planck's law the maximum of the thermal emission is predicted at the wavelength around 10 mm (wavenumber: 1000 cm^{-1}). Although the thermal infrared corresponds to the wavelength region from about 3 mm to 100 mm (about 100–3000 cm^{-1}), but there is actually no strict limit, in particular at longer wavelengths. The Earth's thermal emission presents during day and night. The thermal infrared is also a part of the solar spectrum and thus can be exploited for satellite measurements that operate in solar occultation mode [1]. Today, since many types of radar absorbing materials are commercially available and, the most cost effective means of shielding radar radiation, controlling electromagnetic interference and dissipating electrostatic charge is to use magnetic or dielectric fillers [2,3] or intrinsically conducting polymers [4–7]. Conductive polymers by having conjugated double bonds have important roles in creating the electric current and in the absorption of electromagnetic waves are also very effective. Recently, ferromagnetic and ferroelectric-conducting polymer composites have received considerable attention, especially in studies of composite materials with different types of ferromagnetic or ferroelectric fillers. The main challenge is to design a certain structure, with greatest effect on the magnetic and dielectric properties. The materials used as microwave absorbers can have high magnetic and electric loss due to interaction between the magnetization and electric polarization [2,8]. Currently in this field there is interest in the use of magnetoelectric-based microwave absorbing material and provide absorption over a wide bandwidth. Composite materials consisting of magnetic media and electronic media are known as

* Corresponding author.
E-mail address: shhosseini@iiau.ac.ir (S.H. Hosseini).

http://dx.doi.org/10.1016/j.jallcom.2015.05.099
0925-8388/

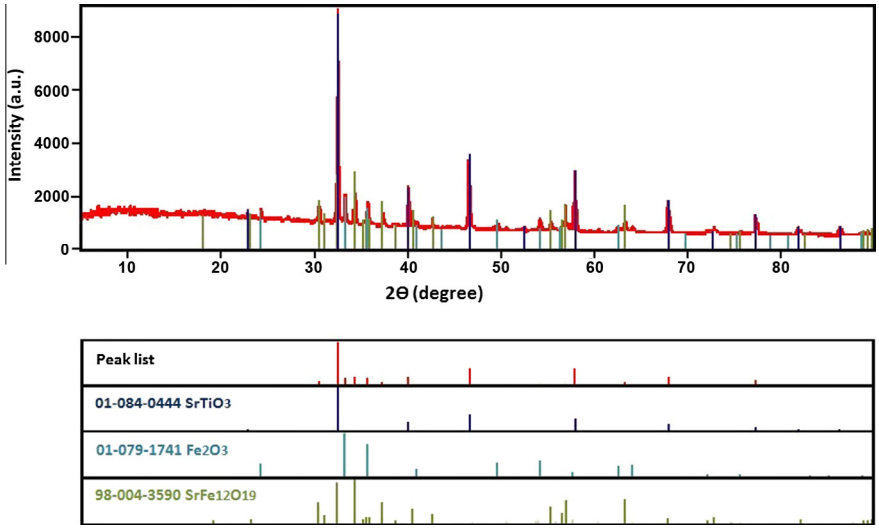

Fig. 1. XRD patterns for $SrTiO_3/SrFe_{12}O_{19}$/PANI nanocomposite.

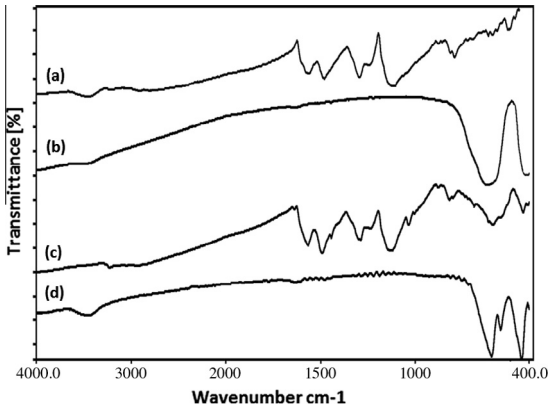

Fig. 2. FT-IR spectra for the (a) PANI, (b) $SrTiO_3$, (c) $SrTiO_3/SrFe_{12}O_{19}$/PANI (50 wt%) and (d) $SrFe_{12}O_{19}$.

magnetoelectric composites. These composites have magnetoelectric effects and electromagnetic properties that are absent in their constituent phases [2,9–11]. The current studies are aimed to changes mass weight and shape for the microwave absorption materials, especially the ferrite materials [12–14]. $BaTiO_3$ and $BaFe_{12}O_{19}$ show various electrical and magnetic properties, such as the complex permeability and the complex permittivity. Particularly they are important in determining their high frequency characteristics. So, infrared and microwave absorbing properties of $BaTiO_3$/polyaniline and $BaFe_{12}O_{19}$/polyaniline composites were investigated by Wu, too [15]. Recently, nonconducting infrared-absorbing thin films were prepared by black silicon and bismuth by Li and Gradhand [16,17]. As they show an IR absorbance in the 3–15 μm wavelength range. The gold nanoparticles and nanophase zinc ferrite have been used as near and far-infrared light absorbing materials [18,19].

Within this work, we have synthesized some papers of microwave absorbing materials [2,4,7,10,20] and X-ray [21] attenuation based on conducting polymers and nanoparticles. Although some other works on such composites have been reported in recent years, but there is no report neither on the microwave nor infrared as multi absorbers by core–shell structure. In this research, we have tried to make such materials with special interest because they are either microwave absorbing performance or infrared stealth properties.

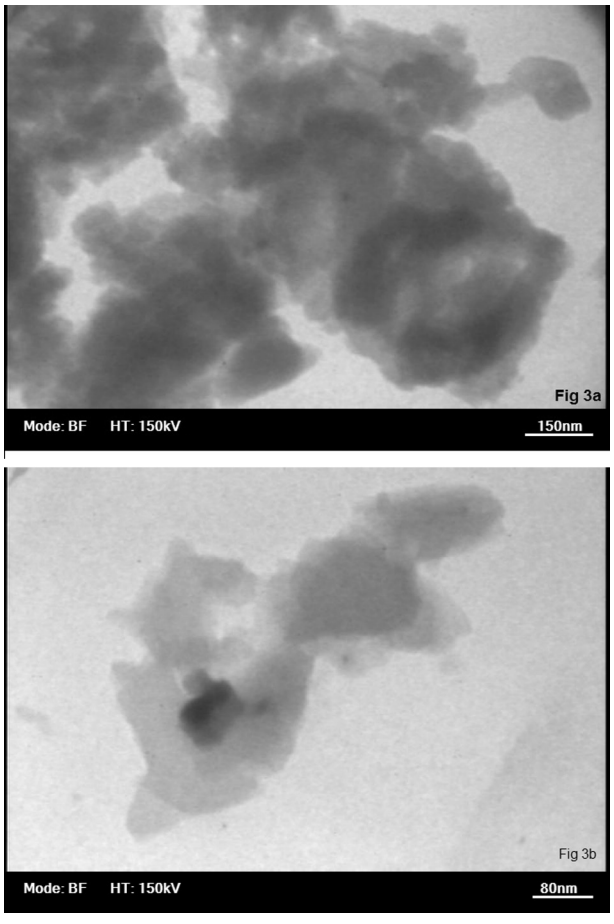

Fig. 3. TEM images of the $SrTiO_3/SrFe_{12}O_{19}$/PANI nanocomposite with different scales.

2. Experiment

2.1. Materials

All the reagents that have been used in this experiment, purchased from Merck, including $TiCl_4$ (99.9%, Acros Organics), $SrCl_2{\cdot}6HO$, $Ba(NO_3)_2$, $Sr(NO_3)_2$, $Fe(NO_3)_3{\cdot}9H_2O$, $FeCl_3{\cdot}6H_2O$, KOH, dodecylbenzenesulfonic acid (DBSA), polyoxyethylene (20) sorbitan monooleate (Tweent80), citric acid, ammonia persulfate

(APS), methyl methacrylate, methanol, benzoyl peroxide, toluene and ammonia (NH_3). Other chemicals were of analytical grade used without further purification. Distilled and deionized water also used through the work. Aniline monomer (analytical grade, Merck) distilled twice under reduced pressure and stored below 0 °C.

2.2. Preparation of polymethyl methacrylate (PMMA)

50 mL of methyl methacrylate as monomer was added in 50 mL toluene in 250 mL flask and gets deoxidized by nitrogen gas. Then 0.8 g of benzoyl peroxide as an initiator was solved in 15 mL toluene and added to above solution. It was refluxed under N_2 gas for 2 h. The PMMA was precipitated in ice methanol and dried.

2.3. Preparation of $SrTiO_3$ nanoparticles

An aqueous solution of strontium and titanium oxide was obtained by mixing 14.66 g $SrCl_2{\cdot}6H_2O$ in 40 mL deionized water and 3.79 g $TiCl_4$ in 40 mL chilled deionized water. One-half-gram of polyoxyethylene (20) sorbitan monooleate (Tweent 80) was added as the surface modifier to the above solution. The solution pH raised to 13.5 by drop wise adding 4 M KOH with stirring, resulting in a white colloidal sol. The final volume was adjusted to 100 mL using deionized water, and then, 25 mL of the sol was transferred to a 30 mL stainless steel vessel. The sealed vessel was heated to 230 °C for 0.5–2 h. After cooling down to the room temperature, the resultant precipitate was centrifuged and washed with water for several times, and finally dried at 60 °C for 24 h in a vacuum oven. Excess Sr^{2+} and KOH were removed during washing [22].

2.4. Synthesis of $SrTiO_3/SrFe_{12}O_{19}$ nanoparticles (50/50% w/w)

First strontium titanate was dispersed and prepared in deionized water as core and ultrasonic vibration for 20 min. According to the formula of $SrFe_{12}O_{19}$, the stoichiometric amounts of $Sr(NO_3)_2$ and $Fe(NO_3)_3{\cdot}9H_2O$ were dissolved into deionized water by adding of citric acid. The pH value of the solution was adjusted to 7.0 with appropriate ammonia solution. The green solution was evaporated slowly at 80 °C until a little of sol remained. Then the PMMA was added into the precursor sol. After ultrasonic vibration for 10 min, the mixed solution was still evaporated at 70 °C until a viscous gel formed. The viscous gel was then dried at 110 °C. They were directly calcined at 850 °C for 1 h without the course of ignition and grinding under vacuum.

2.5. Synthesis of $SrTiO_3/SrFe_{12}O_{19}$/PANI nanocomposites

$SrTiO_3/SrFe_{12}O_{19}$/PANI as multi core–shell nanocomposites was prepared by in situ polymerization in the presence of DBSA as the surfactant and dopant and APS as the oxidant. The 0.1 g DBSA dissolved in distilled water with vigorous stirring for about 20 min. The $SrTiO_3/SrFe_{12}O_{19}$ nanoparticles added to the DBSA solution under stirring condition for approximately 1 h. Then 1 mL of freshly distilled aniline as monomer added to the suspension and stirred for 30 min. The $SrTiO_3/SrFe_{12}O_{19}$ nanoparticles were dispersed well in the mixture of aniline/DBSA under ultra sonication for 2 h. 3.28 g APS as initiator dissolved in 60 mL deionized water and added drop wise to the stirred reaction mixture. Polymerization was allowed to proceed while stirring in an ice-water bath for 6 h. The nanocomposite was obtained by filtering and washing the suspension with deionized water and ethanol, respectively. The obtained dark-green powder contains $SrTiO_3/SrFe_{12}O_{19}$/PANI (with different weight ratio) and dried under vacuum for 24 h.

2.6. Characterization

The ultrasonic experiments were carried out by an ultrasonic disperser (BANDELIN sonorex digitec, 35 kHz, Germany). The XRD patterns of the samples were collected on a Philips-PW1800 with Cu Kα radiation (λ = 1.54184 Å) in the 2θ = 4–90° with steps of 0.02°, scanning operated at 40 kV and 30 mA (Netherland). Field emission scanning electron microscopes (FESEM) were performed by Hitachi S-4160 model (Japan) to observe the surface morphologies of the nanoparticles. The morphologies of as prepared samples were examined with transmission electron microscopy (TEM) by ZWISS-EM900, (Germany). Samples of TEM were prepared by dispersing the final nanoparticles in ethanol; the suspension was then dropped on copper grids. The magnetic measurements carried out at room temperature using a IRI-Kashan vibrating sample magnetometer (VSM) with a maximum magnetic field of 10 kOe (Research Institute NanoTechnology of Kashan – Iran). Microwave absorption properties of nanocomposites were measured using

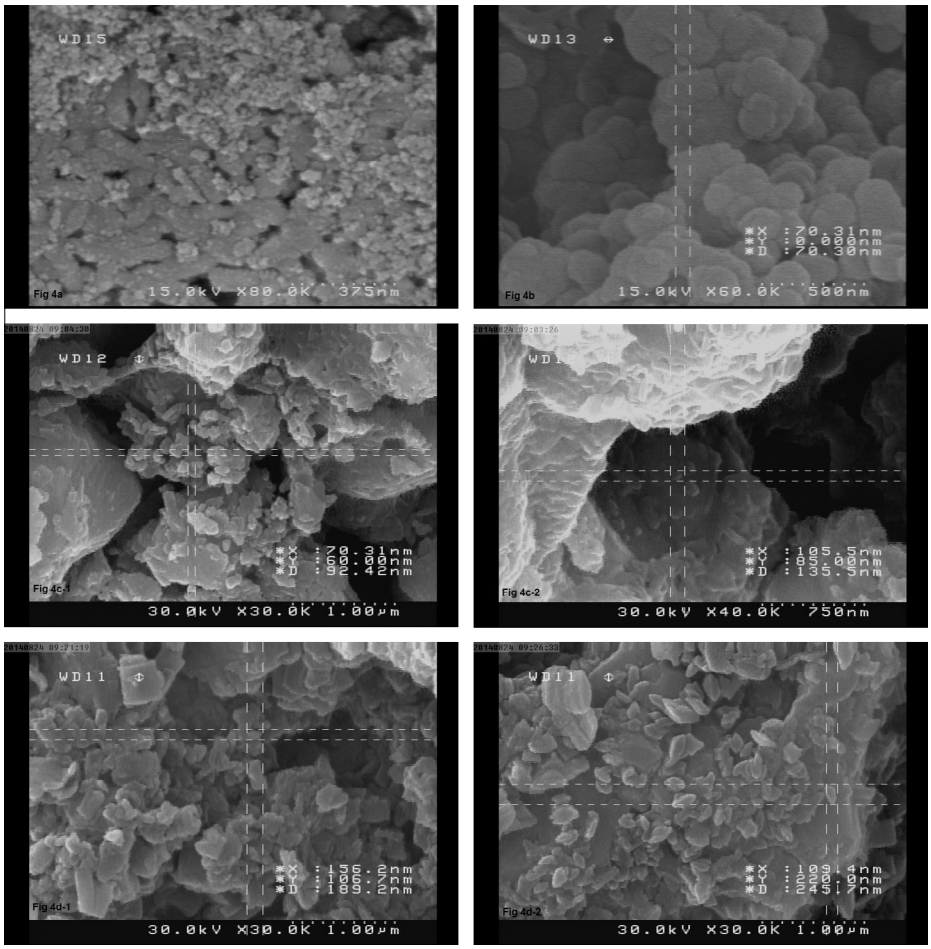

Fig. 4. FE-SEM images of (a) $SrTiO_3$, (b) $SrFe_{12}O_{19}$, (c and c′) $SrTiO_3/SrFe_{12}O_{19}$ and (d and d′) the $SrTiO_3/SrFe_{12}O_{19}$/PANI nanocomposite.

microwave vector network analyzer (Agilent technologies Inc. 8722-USA) in the 8–12 GHz range at room temperature. The electrical conductivity of compressed pellets of polymers and nanocomposites was measured using a standard four-probe set-up connected to a Keithley system comprising a voltmeter and a constant high-current source, made in IRAN. The Thermal IR absorption properties of the nanocomposites were measured by Thermal camera (Rs-D780 B).

3. Results and discussion

3.1. XRD data

Fig. 1 shows XRD patterns for $SrTiO_3/SrFe_{12}O_{19}$/PANI (50 wt%) nanocomposites. The exhibited peaks can be indexed as cubic lattice of $SrTiO_3$ and the calculated lattice constants which are in good agreement with the tabulated values (a = 3.1912 Å; JCPDS cards no. 01-084-0444). By comparing to the standard XRD pattern of the $SrTiO_3$ powder, the peaks at 2θ = 32.3, 39.9, 46.5, 52.1, 57.8 and 67.9 can be attributed to the Miller indices of (110), (111), (200), (210), (211), and (220). According to Fig. 1, hexaferrite $SrFe_{12}O_{19}$ nanoparticles have been obtained. It is clearly seen that all peaks (2θ = 30.2, 32.2, 34.2, 55.4, 56.9, 63.1) correspond to the characteristic peaks of hexagonal-type lattice of $SrFe_{12}O_{19}$ (JCPDS file no. 98-004-3590). However, it should be noticed that there are some peaks of α-Fe_2O_3 in the XRD pattern of $SrFe_{12}O_{19}$ nanoparticles. The average crystallite size can be calculated by the Debye–Scherrer formula: $D = 0.89\lambda/\beta \cos\theta$ where λ is the wavelength of Cu Kα radiation and the value of K depends on several factors, including the Miller index of reflection plane and the shape of the crystal. If the shape is unknown, K is often assigned as a value of 0.89, D is the average crystallite size, θ is the Bragg's angle, and β is the full width at half-maximum of the diffraction peaks. From the obtained peak width of XRD patterns, the average crystallite sizes of $SrTiO_3$ and $SrTiO_3/SrFe_{12}O_{19}$ can be calculated to be 31.66 and 65.54 nm, respectively. The XRD pattern in Fig. 1 indicates that $SrTiO_3/SrFe_{12}O_{19}$/PANI core–shell structure has semi-crystalline shape.

3.2. FTIR spectroscopy

Fig. 2(a–d) shows FTIR spectra for nanocomposite (a) PANI, (b) $SrTiO_3$, (c) $SrTiO_3/SrFe_{12}O_{19}$/PANI (50 wt%) and (d) $SrFe_{12}O_{19}$. FTIR spectrum of PANI was showed in Fig. 2a. The peak at 796.65 cm^{-1} is attributed to the p-di-substituted aromatic ring C—H out of plane bending. The specific peaks around 1106.65 cm^{-1} is associated with vibrational modes of N=Q=N (Q refers to the quinonic type rings), indicating that PANI is formed in our sample. The peak at 1296.61 cm^{-1} is corresponded to N—H bending. The peaks at 1563.62 and 1481.61 cm^{-1} are assigned to the characteristic C=C and C—N stretching of the quinoid and benzenoid rings of PANI. As they shown in Fig. 2(b–d), the observed peaks under 650 cm^{-1} are related to metal–oxide vibration bands. Fig. 2b and d illustrates the infrared spectra of $SrTiO_3$ and $SrFe_{12}O_{19}$. The observed peaks at 623.36 and 599.8 are attributed to vibration stretching modes of Ti—O in $SrTiO_3$ and Fe—O in $SrFe_{12}O_{19}$, respectively. The peaks at 400 and 442 cm^{-1} are related to vibration stretching modes of Sr—O in both. Fig. 2c shows an FTIR spectrum for $SrTiO_3/SrFe_{12}O_{19}$/PANI (50 wt%). The observed peaks at 432.5 and 591.45 cm^{-1} can be assigned to the vibration stretching modes of Sr—O and Fe—O, respectively. The peak at 1038.45 cm^{-1} is attributed to the symmetric and anti-symmetric stretching vibrations of SO_3 group of dopant (DBSA). The specific peak around 1125.35 cm^{-1} is associated with vibrational modes of N=Q=N (Q refer to the quinonic type rings), indicating that PANI is formed in our sample. The peaks at 1290.39 and 1125.35 cm^{-1} correspond to N—H bending and asymmetric C—N vibrational stretching of the benzenoid rings, respectively. The peaks at 1492.34 and 1568.37 cm^{-1} are attributed to C=N and C=C stretching of the PANI ring (similar to a benzoidal structure). In addition the bands at 2915.30 and 3225.29 cm^{-1} correspond to the symmetric stretching vibration of C—H aliphatic group of dopant (DBSA) and O—H, N—H stretching modes. According to the mentioned data, it is inferred that the claimed nanocomposite has been successfully synthesized.

3.3. TEM analysis

Fig. 3(a and b) shows a TEM images of the $SrTiO_3/SrFe_{12}O_{19}$/PANI nanocomposite. The average nanoparticles ($SrTiO_3/SrFe_{12}O_{19}$) size as core is estimated to be 60 nm. This particle size is in accordance with the calculated value with Debye–Scherrer formula, which was about 65.54 nm. These particles are polydisperse, and some of them form multi particle aggregates due to the magneto-dipole interparticle interactions. It is clear that a PANI coating layer is wrapped around the $SrTiO_3/SrFe_{12}O_{19}$ surface, forming a core–shell structure for the $SrTiO_3/SrFe_{12}O_{19}$/PANI nanocomposite. The dark region is the magnetic $SrTiO_3/SrFe_{12}O_{19}$ core and the gray area is the PANI shell; these colors differences arise because of differing electron penetrability.

3.4. SEM images

Fig. 4(a–d) shows SEM images of (a) $SrTiO_3$, (b) $SrFe_{12}O_{19}$, (c and c′) $SrTiO_3/SrFe_{12}O_{19}$ nanoparticles and (d and d′) $SrTiO_3/SrFe_{12}O_{19}$/PANI multi core–shell nanocomposite. From the image, it can also be seen that the uncoated $SrTiO_3$ and $SrFe_{12}O_{19}$ nanoparticles are about 25–35 and 39 nm, whereas the $SrTiO_3/SrFe_{12}O_{19}$ core/shell particles are about 70–110 nm. Fig. 4 shows clearly that the particles were

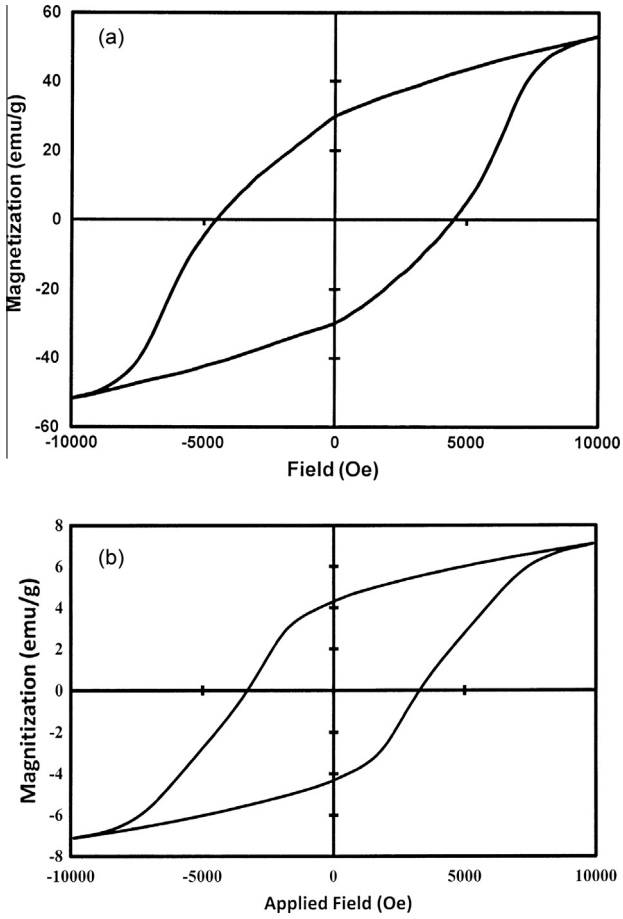

Fig. 5. Field-dependent magnetization curves of (a) $SrFe_{12}O_{19}$ and (b) $SrTiO_3/SrFe_{12}O_{19}$/PANI nanocomposites.

Table 1
The electrical conductivity of $SrTiO_3/SrFe_{12}O_{19}$/PANI nanocomposites.

Sample	Conductivity (S/cm)
PANI	0.015
$SrTiO_3/SrFe_{12}O_{19}$ 20 wt%	8.5×10^{-3}
$SrTiO_3/SrFe_{12}O_{19}$ 50 wt%	2.3×10^{-4}
$SrTiO_3/SrFe_{12}O_{19}$ 80 wt%	6.5×10^{-5}

sponge-shaped. Fig. 4d and d′ shows the images of $SrTiO_3/SrFe_{12}O_{19}$/PANI multi core–shell particles with an average diameter of 100–180 nm. An assumption can be drawn as follow: in $SrTiO_3/SrFe_{12}O_{19}$ and $SrTiO_3/SrFe_{12}O_{19}$/PANI multi core–shell nanoparticles.

3.5. Vibrating sample magnetometer (VSM)

Magnetic properties of $SrFe_{12}O_{19}$ and $SrTiO_3/SrFe_{12}O_{19}$/PANI were measured at the room temperature with a VSM with an applied field $-10\ kOe \leqslant H \leqslant 10\ kOe$. The hysteresis loops of are illustrated in Fig. 5(a and b). The $SrTiO_3/SrFe_{12}O_{19}$/PANI nanocomposites consist of one magnetic phases, the hysteresis loop shows a single-phase–like behavior, and the magnetization changes that happen smoothly with the applied field. This indicates that the $SrTiO_3/SrFe_{12}O_{19}$ as the core and PANI as the shell contact intimately. For each sample, the magnetic parameters such as saturation magnetization (M_s), coercivity (H_c) and remnant magnetization (M_r) determined by the hysteretic loops are measured. As shown in Fig. 5(a and b), it is also clear, that the value of M_s. and M_r. decreases from 57 and 30 emu/g for $SrFe_{12}O_{19}$ to 6.8 and 4.3 emu/g for the core–shell structure nanocomposites owing to the coating of PANI. H_c was decreased from 4506 Oe for $SrFe_{12}O_{19}$ to 3000 Oe for $SrTiO_3/SrFe_{12}O_{19}$/PANI. When PANI is added for the formation of multi core–shell structure, the magnetic properties were decreased by increasing conductivity. VSM curve of $SrTiO_3/SrFe_{12}O_{19}$/PANI nanocomposite showed that ferromagnetic behavior.

3.6. Conductivity

Electrically conductivity of samples at room temperature was measured by four probe method. The conductivity of PANI after polymerization by APS as initiator and DBSA as dopant is 0.015 S/cm. When mass content of $SrTiO_3/SrFe_{12}O_{19}$ nanoparticles were incorporated, the conductivity of $SrTiO_3/SrFe_{12}O_{19}$/PANI nanocomposite with different weight ratios were reduced sharply. The decrease in conductivity of $SrTiO_3/SrFe_{12}O_{19}$/PANI composites, by $SrTiO_3/SrFe_{12}O_{19}$ in the core of the nanoparticles may be attributed to the insulting behavior of the ferrite and partial blockage of the conductive path. All conductivities summarized in Table 1.

3.7. Thermal infrared absorption study

Thermal infrared is a part of the solar spectrum with a broad band of energy. For infrared-thermal application such as infrared thermal detectors, thermal imaging, a strong infrared absorber that operating over the entire wavelength bandwidth is desired. Metal film can be a wide-band absorber for infrared radiation with a very small heat capacity, in compare with previous methods like

Table 2
The light reflectivity times (s) again of $SrTiO_3/SrFe_{12}O_{19}$/PANI in different weight ratios ($SrTiO_3/SrFe_{12}O_{19}$ as core) and thicknesses on metallic disks.

$SrTiO_3/SrFe_{12}O_{19}$/PANI (wt% core)	Thickness (mm)		
	1	1.5	2
20	3	4	5
40	3.5	5	7
60	5	8	10
80	6	10	13

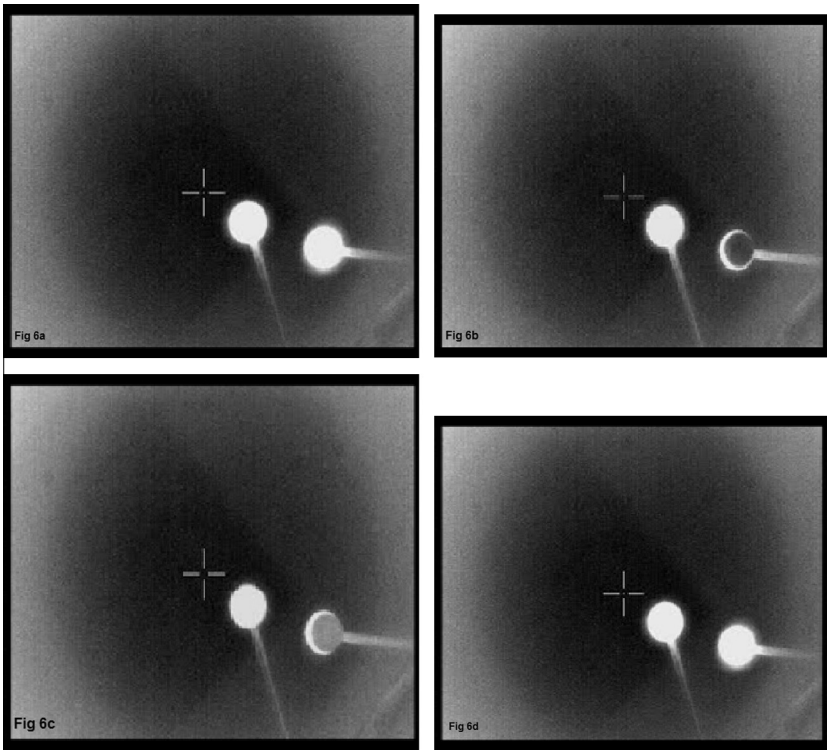

Fig. 6. Thermal IR images of $SrTiO_3/SrFe_{12}O_{19}$/PANI nanocomposites in different weight ratio and thickness at (a) without sample, (b) with sample (left is reference and right is sample), (c) during of test and (d) end of test (light reflectivity again) on metallic disks.

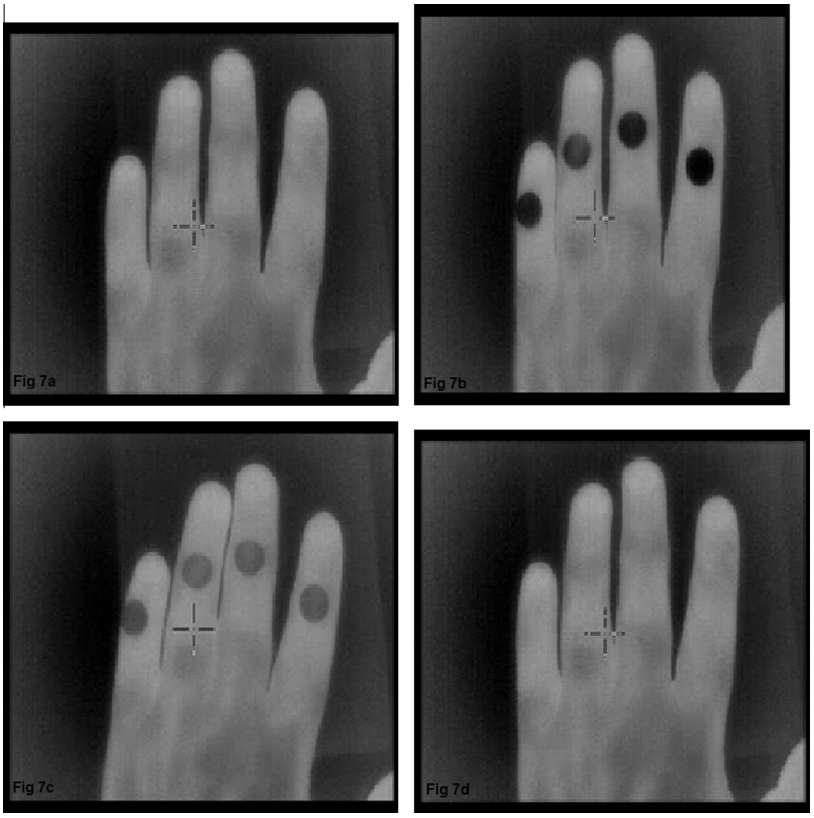

Fig. 7. Thermal IR images of $SrTiO_3/SrFe_{12}O_{19}$/PANI nanocomposites in different weight ratio and thickness at (a) without samples, (b) with sample (20, 40, 60 and 80 wt%), (c) during of test and (d) end of test (light reflectivity again) on human hand.

Table 3
Relative light reflectivity times (min) again of $SrTiO_3/SrFe_{12}O_{19}$/PANI in different weight ratios ($SrTiO_3/SrFe_{12}O_{19}$ as core) and thicknesses on human hand.

$SrTiO_3/SrFe_{12}O_{19}$/PANI (wt% core)	Thickness (mm)		
	1	1.5	2
20	15	25	32
40	30	43	51
60	50	–	–
80	–	–	–

Table 4
Surface temperature (°C) of $SrTiO_3/SrFe_{12}O_{19}$/PANI in different weight ratios ($SrTiO_3/SrFe_{12}O_{19}$ as core) and thicknesses on human hand after 30 min (human temperature; 37 °C).

$SrTiO_3/SrFe_{12}O_{19}$/PANI (wt% core)	Thickness (mm)		
	1	1.5	2
20	35.8	35.3	35.1
40	35.0	34.5	33.8
60	34.2	33.8	33.6
80	33.8	33.2	31.8

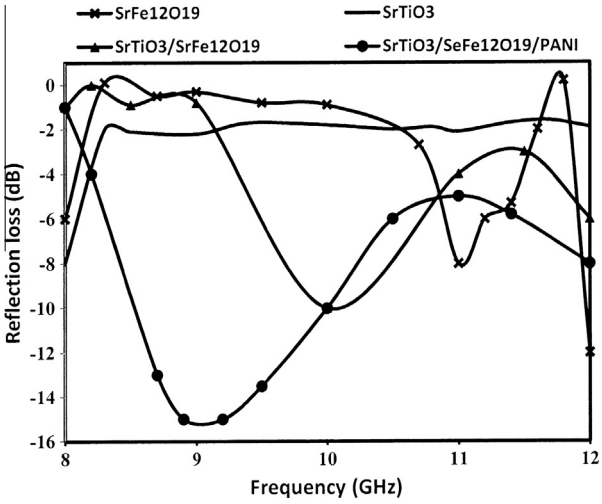

Fig. 8. Frequency dependence of RL for the $SrTiO_3$, $SrFe_{12}O_{19}$, $SrTiO_3/SrFe_{12}O_{19}$ and $SrTiO_3/SrFe_{12}O_{19}$/PANI nanocomposites.

intrinsic absorber, black coatings, multilayer absorbers or metal dielectric composite [23]. But polymeric nanocomposites with multi core shell structure have not yet been reported. Here, first, a few metallic disks with 13 mm diameter and 20 cm holder were made. So, all samples in different weight ratios and thicknesses were prepared with 13 mm diameter, too. The metallic disks were heated to 40 °C and then samples put on it. The thermal IR images of $SrTiO_3/SrFe_{12}O_{19}$/PANI nanocomposites in different weight ratio and thickness are shown in Fig. 6(a–d). Table 2 shows results in this study.

All metals have high thermal transmission coefficient and low light reflectivity times. On the other hands, thermal IR tests to be continued on human hand. Human hand have low thermal transmission coefficient and thus is suitable for these tests. Fig. 7(a–d) shows thermal IR images for $SrTiO_3/SrFe_{12}O_{19}$/PANI nanocomposites in different weight ratios and thicknesses. The result is summarized in Table 3.

Table 5
Microwave absorption behavior of $SrTiO_3$, $SrFe_{12}O_{19}$ and $SrTiO_3/SrFe_{12}O_{19}$ nanoparticles and $SrTiO_3/SrFe_{12}O_{19}$ /PANI nanocomposites.

Sample	Frequency (GHz)	Reflection loss (db)
$SrTiO_3$	8	−8
	8.3	−2
	10.5	−2
	12	−1.9
$SrFe_{12}O_{19}$	8	−6
	8.5	0.1
	9	−0.7
	11	−8
	11.8	0.2
	12	−12
$SrTiO_3/SrFe_{12}O_{19}$	8	−1
	10	−10
	11.5	−3
	12	−6
$SrTiO_3/SrFe_{12}O_{19}$/PANI	8	−1
	8.9	−15
	11	−5
	12	−8

As results show, light reflectivity times of samples on human body are higher than metallic disks. So, they are suitable choice for thermal IR as absorbers. The light reflectivity times of samples were optimized by increasing the weight ratio as well as the thickness.

The Surface temperature of samples was measured by using leaser thermometer for 30 min and the result is summarized in Table 4. As Table 4 results show, the human temperature cannot transmit to the samples by increasing weight ratio of the core. Therefore the weight ratio ($SrTiO_3/SrFe_{12}O_{19}$ as core) above 40% and 1 mm diameter are the best results as thermal IR absorber.

3.8. Microwave absorbing study

The difference in microwave absorbing properties of different composites are related to the electric and magnetic loss that are generated by the magnetoelectric effects and by the changes of boundary condition of the microwave field at the interface between the polycrystalline particles and PANI polymer. In this work, we improved magnetoelectric effects and microwave absorbing properties using tablet form with 13 mm diameter and 1 mm thickness as the test sample. The microwave absorbing properties of the nanocomposite with the coating thickness of 1 mm investigated by using vector network analyzers in the frequency range of 8–12 GHz. The results for $SrTiO_3$, $SrFe_{12}O_{19}$ and $SrTiO_3/SrFe_{12}O_{19}$ nanoparticles and $SrTiO_3/SrFe_{12}O_{19}$/PANI nanocomposites are shown in Fig. 8 and summarized in Table 5. Comparison of data for $SrTiO_3/SrFe_{12}O_{19}$ and $SrTiO_3/SrFe_{12}O_{19}$/PANI reveals that PANI increased the absorption as well as the electrical conductivity. The absorption bandwidth under −10 dB is 1.6 GHz ranging from 8.4 to 10 GHz. for $SrTiO_3/SrFe_{12}O_{19}$/PANI.

4. Conclusion

The $SrTiO_3/SrFe_{12}O_{19}$/PANI nanocomposites were well defined in size and shape and exhibited good electrical conductivity. The light reflectivity times of samples on human body are higher than metallic disks. So, they are suitable for thermal IR absorbers. The light reflectivity times of samples were increased by increasing weight ratio and thickness. Human temperature could not transmit to samples by increasing weight ratio of core. Therefore weight ratio ($SrTiO_3/SrFe_{12}O_{19}$ as core) above 40% and 1 mm diameter are the best result as thermal IR absorber. The $SrTiO_3/SrFe_{12}O_{19}$/PANI enhanced broad band infrared light absorption was observed in the wavelength range of 10–40 μm. A minimum RL of −15 dB was observed at 9.2 GHz for a 1 mm thickness nanocomposite. The application of these samples may improve the IR thermographic detection, catalysis, sensors, magnetic data storage, electromagnetic resonance wave absorption, photonic crystals, and microelectronic devices and military aspects.

References

[1] J.P. Burrows, C. Clerbaux, J.R. Drummond, J.M. Flaud, J. Orphal, The Remote Sensing of Tropospheric Composition from Space, Chapter 3: Thermal Infrared: Absorption and Emission-Trace Gases and Parameters, Springer Verlag Book, 2011.
[2] S.H. Hosseini, M. Moloudi, Synth. React. Inorg., Met.-Org., Nano-Met. Chem. 43 (6) (2013) 671.
[3] Z.G. Fan, G.H. Luo, Z.G. Zhang, L. Zhou, F. Wei, Mater. Sci. Eng. B 132 (2006) 85.
[4] S.H. Hosseini, S.H. Mohseni, A. Asadnia, H. Kerdari, J. Alloys Comp. 509 (2011) 4682.
[5] M.A. Soto-Oviedo, O.A. Araújo, R. Faez, M.C. Rezende, M.A. DePaoli, Synth. Met. 156 (2006) 1249.
[6] S.H. Hosseini, R. Rahimi, H. Kerdari, Polym. J. 43 (2011) 745.
[7] S.H. Hosseini, A. Asadnia, J. Nanomater. 2012 (2012) 1.
[8] H.M. Xiao, X.M. Liu, S.Y. Fu, Compos. Sci. Technol. 66 (2006) 2003.
[9] Y.K. Fetisov, A.A. Bush, K.E. Kamentsev, G. Srinivasan, Solid State Commun. 132 (5) (2004) 319.
[10] S.H. Hosseini, A. Asadnia, Int. J. Phys. Sci. 8 (22) (2013) 1209.
[11] S.L. Kadam, C.M. Kanamadi, K.K. Patankar, B.K. Chougule, Mater. Lett. 59 (2005) 215.
[12] X. Huang, J. Zhang, S. Xiao, G. Chen, J. Am. Ceram. Soc. 97 (5) (2014) 1363.
[13] G. Li, L. Wang, W. Li, Y. Xu, RSC Adv. 5 (11) (2015) 8248.
[14] X. Huang, J. Zhang, M. Lai, T. Sang, J. Alloys Comp. 627 (2015) 367.
[15] C.C. Yang, Y.J. Gung, W.C. Hung, T.H. Ting, K.H. Wu, Compos. Sci. Technol. 70 (2010) 466.
[16] Z. Saifeng, L. Yuan, F. Guojin, Z. Baocheng, X. Shiyi, Z. Lei, Z. Li, Opt. Express 19 (21) (2011) 20462.
[17] M. Gradhand, O. Breitenstein, Rev. Sci. Instrum. 76 (2005) 053702.
[18] C. Kojima, Y. Umeda, A. Harada, K. Kono, Colloids Surf., B 81 (2010) 648.
[19] M. Thomas, K.C. George, Indian J. Pure Appl. Phys. 47 (2009) 81.
[20] S.H. Hosseini, A. Asadnia, M. Moloudi, Mater. Res. Innovations 19 (2) (2015) 107.
[21] S.H. Hosseini, M. Askari, S.N. Ezzati, Synth. Met. 196 (2014) 68.
[22] S.W. Lu, B.I. Lee, Z.L. Wang, W.D. Samuels, J. Cryst. Growth 219 (2000) 269.
[23] C.G. Granqvist, Adv. Mater. (Deerfield Beach Fla.) 15 (21) (2003) 1789.